

Influence of Ce substitution on structure, magnetism, and transport in $\text{Pr}_{0.5-x}\text{Ce}_x\text{Ca}_{0.5}\text{MnO}_3$ ($0.03 \leq x \leq 0.20$): From metamagnetism to a spin-glass state

K. R. Mavani and P. L. Paulose

Department of Condensed Matter Physics and Materials Science, Tata Institute of Fundamental Research, Mumbai 400 005, India

(Received 6 May 2005; revised manuscript received 20 July 2005; published 9 September 2005; corrected 12 September 2005)

We have studied the structural, magnetic, and transport properties of $\text{Pr}_{0.5-x}\text{Ce}_x\text{Ca}_{0.5}\text{MnO}_3$ ($0.03 \leq x \leq 0.20$) manganite system. The Ce substitution is found to induce significant modifications in these properties due to the cation disorder and size effects. With increasing Ce substitution, the structure (space group, $Pnma$) evolves from O' ($b/\sqrt{2} < c < a$) orthorhombic to a quasitetragonal ($b/\sqrt{2} \approx c < a$) symmetry. The low Ce substitution ($x=0.03$ and 0.05) induces successive sharp metamagnetic transitions at low temperatures, whereas a spin-glass-like state emerges with further substitution ($x=0.10, 0.15$, and 0.20). A colossal magnetoresistance is observed in the spin-glass-like state on application of high magnetic fields.

DOI: [10.1103/PhysRevB.72.104421](https://doi.org/10.1103/PhysRevB.72.104421)

PACS number(s): 75.47.Lx, 75.30.Kz

I. INTRODUCTION

The ABO_3 -type perovskite manganites display complex properties arising due to the lattice, magnetic, and charge degrees of freedom.¹⁻³ These manganites have been studied extensively for their magnetic and electronic properties in relation to the parameters like average A -site cationic radius ($\langle r_A \rangle$), A -site cation size disorder (σ^2), and structural distortion.¹⁻⁴ These parameters influence the magnetic transitions, metal-insulator transition and charge-ordering transition. Moreover, the external parameters, such as the magnetic field⁵ and laser or x-ray exposure⁶⁻⁸ are found to induce structural, magnetic, and/or electronic phase transitions in some manganites.

Half-doped manganite systems such as $\text{La}_{0.5}\text{Ca}_{0.5}\text{MnO}_3$, $\text{Nd}_{0.5}\text{Ca}_{0.5}\text{MnO}_3$, and $\text{Nd}_{0.5}\text{Sr}_{0.5}\text{MnO}_3$ show a charge-ordered state at low temperatures. Half-doped $\text{Pr}_{0.5}\text{Ca}_{0.5}\text{MnO}_3$ is a charge exchange (CE) type antiferromagnetic (AF) system with charge-ordering² which can be melted by the application of a strong magnetic field (25 T at 4 K) and the system shows a metamagnetic transition (MMT).⁹ Interestingly, Mn-site substitution drastically reduces the critical field (H_c) required for MMT and induces successive sharp MMTs in this system at low temperatures.¹⁰ Recently it is found that the A -site substitution also induces similar successive sharp MMTs in the charge-ordered systems.^{11,12} The sharp MMTs have been explained as a result of competing magnetic phases and phase separation in manganites.^{13,14} A phase-separated ground state evolves at low temperatures where ferromagnetic domains manifest within an antiferromagnetic matrix. The antiferromagnetic and ferromagnetic phases have different crystallographic structures, giving rise to a strain in the phase-separated state of manganites. The lattice degrees of freedom allow the phase-separated ground state to get accommodated, albeit with a strain. An external parameter such as the magnetic field may perturb the energy balance and induce a ferromagnetic state, where the strain could play a role to influence a sharp MMT. The simulation studies show that the disorder also influences phase separation in the manganites.^{15,16} As studied theoretically by Aliaga *et al.*,¹⁷ the fragility of a CE phase increases with disorder and may

result in a glassy state at low temperatures. Recently, it is experimentally observed that the random potential originating due to the A -site disorder entirely suppresses the long-range order and gives rise to a spin-glass state in small bandwidth systems below 50 K.¹⁸ Furthermore, it is found that the quenched disorder affects the long-range ordered CE state more than the ferromagnetic state.¹⁷

The CE-type antiferromagnetic $\text{Pr}_{0.5}\text{Ca}_{0.5}\text{MnO}_3$ has negligible σ^2 due to a similar size of Pr^{3+} (1.126 Å) and Ca^{2+} (1.12 Å) ions. With a prime objective to investigate the Ce substitution effects on structural, magnetic, and transport properties in the context of varying σ^2 and $\langle r_A \rangle$, we have synthesized and studied $\text{Pr}_{0.5-x}\text{Ce}_x\text{Ca}_{0.5}\text{MnO}_3$ ($0.03 \leq x \leq 0.20$) compounds. The half-doped $\text{Pr}_{0.5-x}\text{Ce}_x\text{Sr}_{0.5}\text{MnO}_3$ system is reported with trivalent state of Ce,¹⁹ whereas in many other manganites, Ce has 4+ valency.²⁰⁻²² Any change in the average valency of A -site cations consequently modifies the valency of magnetic Mn ions in the perovskite manganites, which in turn modifies the properties of the system. Thus, apart from $\langle r_A \rangle$ and σ^2 effects, it is also interesting to investigate the valency of Ce in $\text{Pr}_{0.5}\text{Ca}_{0.5}\text{MnO}_3$ system.

In this paper, the compounds are encoded as “PrCe- $x\%$ ” for the $\text{Pr}_{0.5-x}\text{Ce}_x\text{Ca}_{0.5}\text{MnO}_3$ system.

II. EXPERIMENT

The $\text{Pr}_{0.5-x}\text{Ce}_x\text{Ca}_{0.5}\text{MnO}_3$ ($x=0, 0.03, 0.05, 0.10, 0.15$, and 0.20) compounds were synthesized by the conventional solid state reaction method. High purity (>99.9%) powders of Pr_6O_{11} , CeO_2 , CaCO_3 , and MnO_2 were mixed and ground in stoichiometric proportions. Several heating in the temperature range of 950–1150 °C were performed with intermediate grindings and the pelletized samples were finally sintered at 1350 °C for 24 h. The x-ray diffraction (XRD) data were recorded using a powder diffractometer (X'pert). The magnetization measurements were performed using a vibrating sample magnetometer (Oxford Instruments) and a superconducting quantum interference device magnetometer (Quantum Design). Magnetoresistance is measured up to an applied magnetic field of 14 T in the range of 2–300 K, using

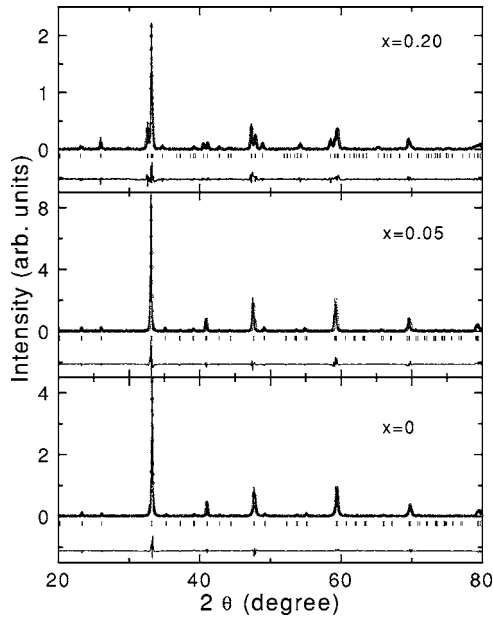


FIG. 1. XRD patterns for $\text{Pr}_{0.5-x}\text{Ce}_x\text{Ca}_{0.5}\text{MnO}_3$ ($0 \leq x \leq 0.20$) with Rietveld fitting. The circles show observed data, the line shows the calculated fit, the Bragg reflections are shown by ticks below the patterns, and the difference between the observed data and the calculated pattern is shown by lines below the ticks.

the physical property measurement system (Quantum Design).

III. RESULTS AND DISCUSSION

A. Structure

The crystal structure of the system is investigated by Rietveld analysis (using the FULLPROF program code) of XRD data. The Rietveld analysis shows that these compounds form in a single phase orthorhombic symmetry with space group: $Pnma$ (No. 62). Figure 1 displays Rietveld fitted XRD patterns of three compounds ($x=0, 0.05$, and 0.20). The XRD peaks split up on substitution of Ce and the splitting increases with x . This may indicate a structural transition from orthorhombic to a monoclinic phase. Also, an orthorhombic to a monoclinic phase transition is earlier observed due to Ce substitution in manganites.²⁰ However, we

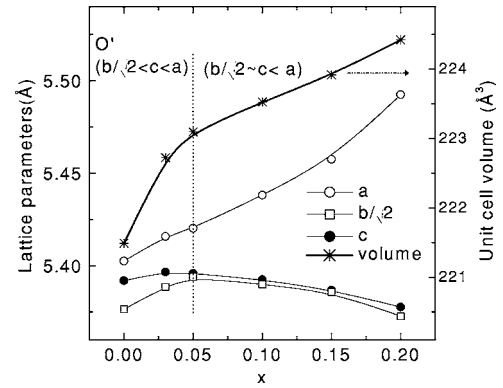


FIG. 2. Variations in lattice parameters and unit cell volume with x in $\text{Pr}_{0.5-x}\text{Ce}_x\text{Ca}_{0.5}\text{MnO}_3$ ($0 \leq x \leq 0.20$).

find that the XRD data of our system do not fit well with the monoclinic symmetry. We have also explored the possibility of a mixed (orthorhombic and monoclinic) phase, but we obtained the best Rietveld fitted patterns for the orthorhombic symmetry. Table I lists the lattice parameters, bond angles, and bond lengths obtained from Rietveld refinements for the $Pnma$ space group. We find that the lattice parameters and unit cell volume vary nonmonotonically with increasing Ce substitution (Fig. 2). Generally, several types of structural distortion are observed in the orthorhombic manganites, like $O^*(b/\sqrt{2} \leq c < a)$, $O''(c \geq a \sim b/\sqrt{2})$, and $O'(b/\sqrt{2} < c < a)$, in different temperature regimes. As is evident from Fig. 2, these samples show a transition from $O'(b/\sqrt{2} < c < a)$ orthorhombic to a quasitetragonal ($b/\sqrt{2} \approx c < a$) symmetry with increasing x . The transformation in the structural symmetry, where lattice parameter “ a ” increases and parameters “ b ” and “ c ” decrease, readily explains the splitting in XRD peaks. The unit cell volume rises with x and varies linearly for $x \geq 0.05$. The Mn–O(1)–Mn bond angle decreases up to $x=0.05$, then it shows a jump at $x=0.10$, and again continues to rapidly decrease with further substitution. It is interesting to note that, while the Mn–O(1)–Mn bond angle is decreasing, the bond length is increasing showing a drop at $x=0.10$. It indicates that there is a correspondence in variation of Mn–O(1)–Mn bond angle with the bond length. We attribute the drastic change in bond angle and bond length at $x=0.10$ to the structural transition in this system. Although the Mn–O(2)–Mn bond angle and average Mn–O(2) bond length do not vary systematically with x , the following cor-

TABLE I. Lattice parameters, unit cell volume, bond angles, bond lengths, average A-site cation radius ($\langle r_A \rangle$) and A-site cation disorder (σ^2) for $\text{Pr}_{0.5-x}\text{Ce}_x\text{Ca}_{0.5}\text{MnO}_3$ compounds.

x	a Å	b Å	c Å	Unit cell volume (Å ³)	Mn–O(1)–Mn (°)	Mn–O(1) (Å)	Mn–O(2)–Mn (°)	$\langle \text{Mn–O}(2) \rangle$ (Å)	$\langle r_A \rangle$ (Å)	σ^2 (10 ⁻³ Å ²)
0	5.403(1)	7.604(1)	5.392(1)	221.5(1)	169.2(2)	1.909(5)	163.4(7)	1.929(20)	1.123	0.009
0.03	5.416(1)	7.621(1)	5.397(1)	222.7(1)	168.7(4)	1.914(2)	153.8(7)	1.963(17)	1.118	0.69
0.05	5.420(1)	7.628(1)	5.396(1)	223.1(1)	165.7(2)	1.922(5)	155.5(6)	1.957(14)	1.115	1.11
0.1	5.438(1)	7.622(1)	5.393(1)	223.5(1)	170.7(1)	1.912(3)	157.8(8)	1.950(21)	1.107	2.11
0.15	5.456(1)	7.617(1)	5.387(1)	223.9(1)	166.2(1)	1.918(2)	150.5(4)	1.983(10)	1.099	2.97
0.2	5.493(1)	7.598(1)	5.378(1)	224.4(1)	145.2(2)	1.991(7)	156.8(5)	1.962(13)	1.092	3.72

relation is observed. With an increase in the Mn–O(2)–Mn bond angle, there is a simultaneous decrease in the average Mn–O(2)–Mn bond length and vice versa. These variations of bond angles are not expected if smaller ions (Pr^{3+}) are replaced by larger ions (Ce^{3+}). However, the nonconforming variations of bond angles and bond lengths are understood by considering the valence state of Ce as tetravalent as discussed below.

There is a difference in the ionic size of $\text{Pr}^{3+}/\text{Ca}^{2+}$ and Ce^{4+} , which reduces $\langle r_A \rangle$. In addition, the Mn^{3+} content is increasing with increasing Ce^{4+} to neutralize the charge. Progressively, the larger Mn^{3+} ions replace smaller Mn^{4+} ions, sharing corners in MnO_6 octahedra. As a combined effect, the average Mn–O–Mn bond angle decreases, while the average bond length and unit cell volume increase. Such peculiar changes in bond angles and bond lengths are also earlier observed in manganites.^{21,23} Although the most stable valence state of Ce is expected to be tetravalent for the air-prepared samples, the possibility of a mixed valent state with a major content of Ce^{4+} ions cannot be ruled out. Since we could find indirect evidence of the tetravalent Ce in this system, the parameters $\langle r_A \rangle$ and $\sigma^2(\sum x_i r_i^2 - \langle r_A \rangle^2)$ are calculated considering Ce^{4+} , for a comparison among these compounds [by using eight coordinate radii for A-site ions reported by Shannon, Acta. Cryst. A 32 751 (1976)]. These parameters are listed in Table I.

B. Magnetization

Figures 3(a)–3(c) display the ac susceptibility (χ_{ac}) at different frequencies as a function of temperature for the samples with $x=0.03, 0.05, 0.10$, and 0.20 . A peak at around ~ 220 K and a shoulder at ~ 150 K are observed in the χ_{ac} curves for PrCe–3% compound [Fig. 3(a)], corresponding to T_{CO} and T_N , respectively. Interestingly, similar features corresponding to T_{CO} and T_N have been observed earlier in magnetization for nearly half-hoped $\text{Pr}_{1-x}\text{Ca}_x\text{MnO}_3$ charge-ordered manganites.²⁴ PrCe–5% also shows a hump at T_N (~ 133 K) and a shoulder corresponding to charge ordering at around 215 K [Fig. 3(a)]. With further substitution of Ce, the χ_{ac} shows a peak at 41, 37, and 35 K, respectively, for PrCe–10%, PrCe–15%, and PrCe–20%, but any feature related to T_N or T_{CO} is absent [Figs. 3(b) and 3(c)]. The magnetization behavior of PrCe–15% resembles that of PrCe–20% compound and is not shown. A small feature is observed at low temperature in χ_{ac} for PrCe–3%, for which we do not know the exact origin at present.

Figures 4(a) and 4(b) display the magnetization isotherms at 2.5 K. PrCe–3% and PrCe–5% show successive sharp MMTs when the magnetic field is increased, and a large irreversibility in the magnetization while the magnetic field is reduced to zero. After the first magnetic field ramp up to 12 T, these samples do not retain the initial magnetic state until warmed up to a temperature around 250 K. Though the H_c is drastically reduced to 5 T for PrCe–3% from 25 T for the undoped compound, it does not attain the expected saturated magnetization ($\sim 3.5\mu_B$ for nearly half-doped manganites). However, with a further increase in substitution up to 5% of Ce, the H_c is reduced to 4.5 T with nearly saturated magne-

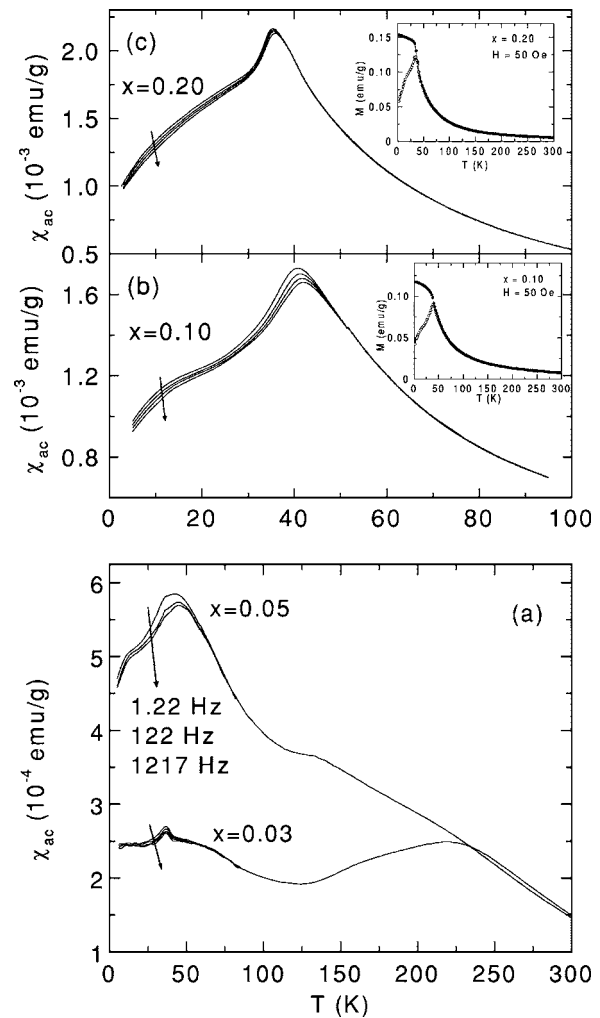


FIG. 3. (a), (b), and (c) χ_{ac} vs temperature at different frequencies (1.22, 12.2, 122, and 1217 Hz) for $\text{Pr}_{0.5-x}\text{Ce}_x\text{Ca}_{0.5}\text{MnO}_3$ ($0.03 \leq x \leq 0.20$) compounds. The increasing frequency is shown by arrows. The insets show magnetization as a function of temperature in ZFC (hollow circles) and FC (solid circles) conditions at 50 Oe.

tization (Fig. 4) at higher fields. The sharp MMTs get smeared out on increasing the temperature to 10 K (Fig. 5). The variation of H_c as a function of temperature for Pr–3% and Pr–5% is shown in Fig. 6. The H_c reduces initially, passes through a minimum, and then keeps rising. The metamagnetic properties of Ce-substituted compounds ($x=0.03$ and 0.05) resemble those¹¹ observed for La^{3+} and Ba^{2+} substituted $\text{Pr}_{0.5}\text{Ca}_{0.5}\text{MnO}_3$. For a comparison, we have shown the variation of H_c for Ba substituted samples from our earlier studies.¹¹ A crossover is observed in H_c variations of PrCe–3% and PrCe–5%, possibly, as a result of the changing $\text{Mn}^{3+/4+}$ ratio with increasing Ce^{4+} content in the system.

In contrast to PrCe–3% and PrCe–5%, the magnetization of PrCe–10%, PrCe–15%, and PrCe–20% does not show any metamagnetic transition up to 12 T. These samples behave like spin glass and it is verified by a strong frequency dependence of ac susceptibility (χ_{ac}) and a large separation in zero-field-cooled (ZFC) and field-cooled (FC) magnetization curves below the peak temperature [Figs. 3(b) and 3(c)]. The

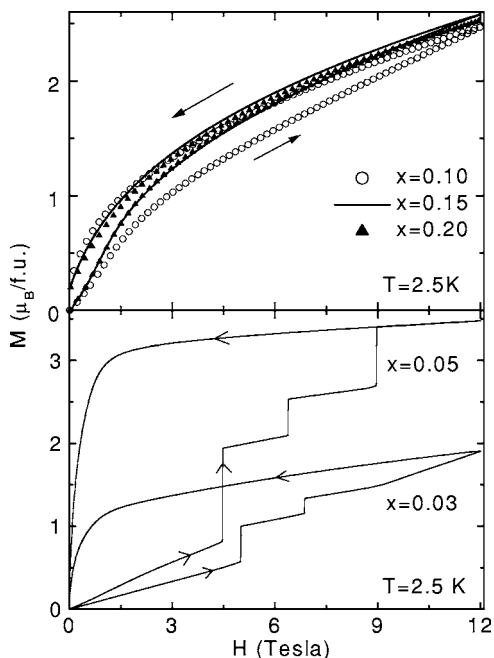


FIG. 4. Magnetization isotherms at 2.5 K for $\text{Pr}_{0.5-x}\text{Ce}_x\text{Ca}_{0.5}\text{MnO}_3$ ($0.03 \leq x \leq 0.20$) compounds. The arrows show the direction of magnetic field ramp.

ac susceptibility peak shifts to higher temperature with increasing frequency. The frequency dependence is observed only around and below the peak temperature (T_G), which indicates that the system homogeneously goes through the spin-glass-like transition. However, such a clear transition is not observed for PrCe-3% and PrCe-5% compounds, but they show a frequency dependence of χ_{ac} below about 60 K [Fig. 3(a)]. This may indicate the presence of some spin-glass component. The magnetic state of these compounds was further probed by measuring the magnetic relaxation at 5 K (Fig. 7). The samples were zero field cooled, then a field of 5000 Oe was applied for 300 s and reduced to zero. The magnetization of PrCe-3% and PrCe-5% shows a weak de-

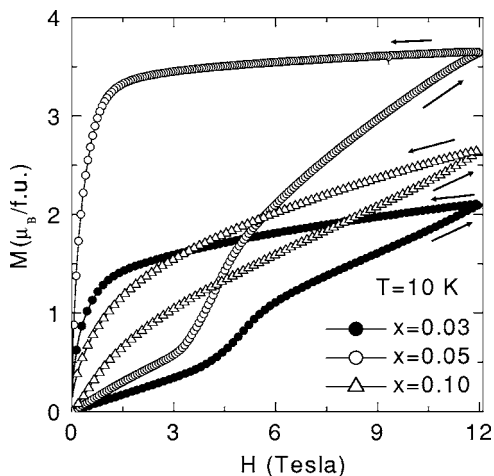


FIG. 5. Magnetization isotherms at 10 K for $\text{Pr}_{0.5-x}\text{Ce}_x\text{Ca}_{0.5}\text{MnO}_3$ ($0.03 \leq x \leq 0.20$) compounds. The arrows show the direction of the magnetic field ramp.

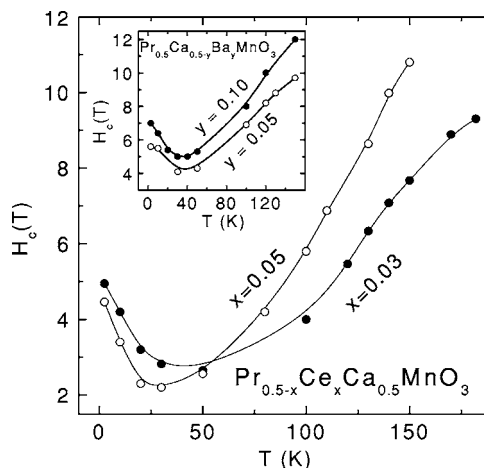


FIG. 6. H_c vs temperature for $\text{Pr}_{0.5-x}\text{Ce}_x\text{Ca}_{0.5}\text{MnO}_3$ ($x=0.03$ and 0.05) compounds. The inset figure shows H_c vs temperature for $\text{Pr}_{0.5}\text{Ca}_{0.5-y}\text{Ba}_y\text{MnO}_3$ ($y=0.05$ and 0.10) compounds.

pendence on time, but the magnetization of PrCe-10%, PrCe-15%, and PrCe-20% compounds shows a strong logarithmic relaxation in the time window of 100 to 7000 s, which further supports the growth of a spin-glass-like state with increasing Ce substitution.

As described above, the $\text{Pr}_{1-x}\text{Ce}_x\text{Ca}_{0.5}\text{MnO}_3$ passes through a structural transition with increasing x and shows a transformation from a robust AF to weak AF (reduced H_c) and finally to a spin-glass-like state. This can be understood in terms of the changing $\text{Mn}^{3+/4+}$ ratio, $\langle r_A \rangle$ and σ^2 as a result of the Ce substitution. The $\text{Mn}^{3+/4+}$ ratio changes with increasing Ce^{4+} and drives the system from a half-doped state to an optimally hole-doped state. Thus, the Mn^{3+} ions replace Mn^{4+} ions and disrupts the alternate zigzag spin arrangement in $\text{Mn}^{3+/4+}$ network of CE type AF phase. A similar scenario is earlier observed for the Cr-doped $\text{Pr}_{0.5}\text{Ca}_{0.5}\text{MnO}_3$ system, where the replacement of Mn ions by Cr ions with reverse magnetic spins destabilizes the CE-type AF state and induces a ferromagnetic phase, coexisting with a charge-ordered

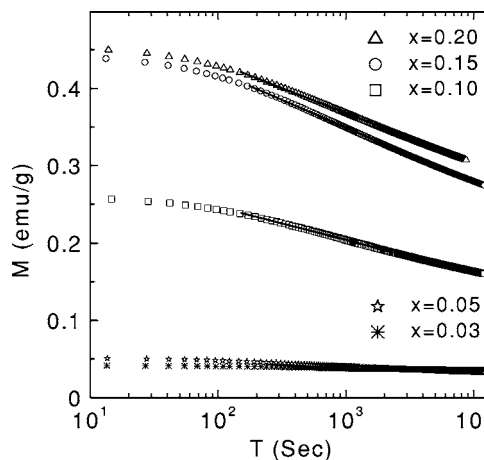


FIG. 7. Magnetic relaxation as a function of time for $\text{Pr}_{0.5-x}\text{Ce}_x\text{Ca}_{0.5}\text{MnO}_3$ ($0.03 \leq x \leq 0.20$) compounds at 5 K. The solid lines show the linear fit.

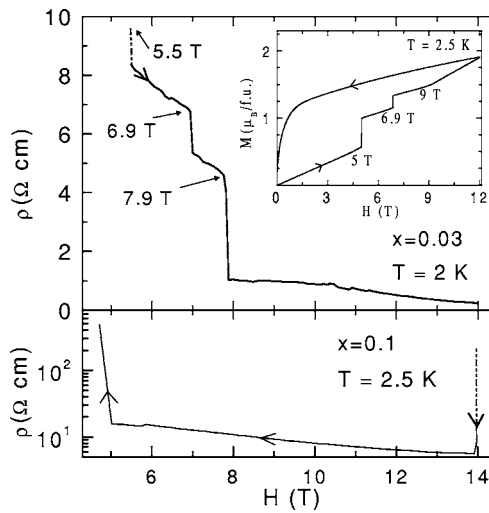


FIG. 8. Resistivity vs the magnetic field for $\text{Pr}_{0.47}\text{Ce}_{0.03}\text{Ca}_{0.5}\text{MnO}_3$ at 2 K and for $\text{Pr}_{0.4}\text{Ce}_{0.1}\text{Ca}_{0.5}\text{MnO}_3$ at 2.5 K. The inset shows the magnetization isotherm for $\text{Pr}_{0.47}\text{Ce}_{0.03}\text{Ca}_{0.5}\text{MnO}_3$ at 2.5 K. The arrows on the curves show the direction of the magnetic field ramp. The dotted lines show a drop in resistivity from high values.

phase.^{25,26} The Ce^{4+} substitution also enhances disorder (σ^2), which could weaken the CE-type charge-ordered state. Thus, as a result of the increasing $\text{Mn}^{3+/4+}$ ratio and σ^2 , a metamagnetic state is induced at much lower H_c than that for the undoped compound. The charge-ordered state melts in steps with multiple metamagnetic jumps, possibly, as a result of the intrinsic structural and magnetoelectronic inhomogeneity in the polycrystalline samples or due to Ce substitution induced local defects.

As per earlier reports, even with optimal hole doping in $(\text{La}, \text{Y})_{1-x}\text{Ca}_x\text{MnO}_3$, $(\text{Tb}, \text{La})_{2/3}\text{Ca}_{1/3}\text{MnO}_3$ and $\text{Tb}_{1-x}\text{Ca}_x\text{MnO}_3$ systems,^{27–29} a small $\langle r_A \rangle$ hinders the ferromagnetic ordering and induces a spin-glass-like state due to competing magnetic interactions. The Ce^{4+} (0.97 Å) ion is smaller than Y^{3+} (1.019) and Tb^{3+} (1.04 Å) ions. The higher Ce^{4+} substitution considerably reduces $\langle r_A \rangle$, drives the system towards an optimally hole-doped state, and also increases the disorder (σ^2). As a combined effect, the system shows a spin-glass-like state.

On comparing the results of the $\text{Pr}_{1-x}\text{Ce}_x\text{Ca}_{0.5}\text{MnO}_3$ system with those¹² of $\text{Pr}_{0.5}\text{Ca}_{0.5-y}\text{Ba}_y\text{MnO}_3$, we find that the results are drastically different for x or $y \geq 0.1$. This provides evidence of tetravalent Ce ions in a $\text{Pr}_{1-x}\text{Ce}_x\text{Ca}_{0.5}\text{MnO}_3$ system as argued in the following way. If Ce would be in a trivalent state then $\langle r_A \rangle$ would increase, as a Ce^{3+} ion is larger than a Pr^{3+} ion. Let us note that the substitution of Ba^{2+} increases $\langle r_A \rangle$ and σ^2 to a greater extent than the Ce^{3+} substitution would have in the $\text{Pr}_{0.5}\text{Ca}_{0.5}\text{MnO}_3$ system. Since the Ba^{2+} substituted system shows metamagnetism within 14 T of an applied magnetic field, Ce^{3+} would also have shown similar results. The contradictory results support the predominantly tetravalent state for Ce.

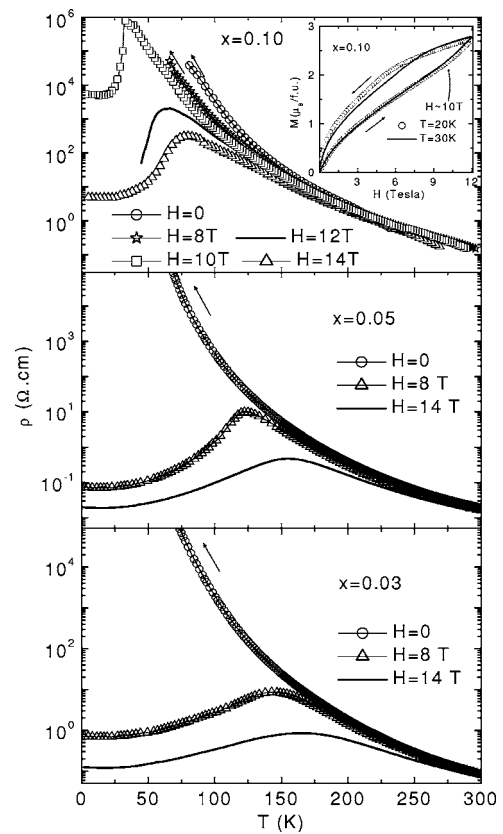


FIG. 9. Resistivity vs temperature for $\text{Pr}_{0.5-x}\text{Ce}_x\text{Ca}_{0.5}\text{MnO}_3$ ($0.03 \leq x \leq 0.10$) compounds in different magnetic fields. The arrows indicate the increasing resistivity beyond 1 MΩ cm. The inset shows magnetization isotherms at 20 and 30 K for the $\text{Pr}_{0.4}\text{Ce}_{0.1}\text{Ca}_{0.5}\text{MnO}_3$ compound.

C. Magnetoresistance

The resistivity as a function of the magnetic field is shown for PrCe–3% and PrCe–10%. The sharp steps in resistivity are observed showing the transition from an insulating to a metallic state. Interestingly, these steps correspond with the sharp magnetization jumps at 2.5 K (inset Fig. 8), indicating a strong correlation between magnetic and electronic transitions in PrCe–3%. The PrCe–5% compound shows a similar behavior. At 2.5 K, PrCe–10% shows a very high resistivity, but on increasing the magnetic field to 14 T, the resistivity drops to about 10 Ω cm, indicating the opening of ferromagnetic channels.

Figure 9 shows resistivity versus temperature for PrCe–3%, PrCe–5%, and PrCe–10% compounds in different magnetic fields. The data are taken while cooling. All the three compounds exhibit insulator-metal (I-M) transitions at high enough magnetic fields. The peak temperature (T_p) corresponding to the I-M transition shifts to higher temperatures with the increase in magnetic field. Surprisingly, an insulator to the metalliclike transition is observed at high magnetic fields ($H \geq 10$ T) for PrCe–10%, which shows a spin-glass-like behavior. Such peculiar magnetoresistance is also observed for single-crystal $\text{Eu}_{0.5}\text{Ba}_{0.5}\text{MnO}_3$ manganite, which is shown to be an atomic level spin glass.¹⁷ According to the

simulation studies by Burgy *et al.*,³⁰ doped transition metal oxides are intrinsically inhomogeneous and due to the disorder effect, they show the coexistence of clusters with different signs of order parameters, separated by thin regions of competing phases. Furthermore, the transition between these phases may be percolative on the application of moderate fields. This can explain the observed magnetoresistance behavior in PrCe-10%; however, a high magnetic field such as 10 T is required to induce the percolation of charge carriers in this spin-glass-like system. We find that PrCe-10% shows an upward trend in magnetization around 10 T between the temperatures 20 and 30 K (inset Fig. 9). This clearly shows a growth of the ferromagnetic phase which is retained down to low temperatures due to the field cooling (the magnetoresistance is measured while cooling). However, in the ZFC condition, a higher magnetic field of 14 T is required to induce the metalliclike state (Fig. 8).

IV. CONCLUSION

With Ce substitution in the $\text{Pr}_{1-x}\text{Ce}_x\text{Ca}_{0.5}\text{MnO}_3$ system, the structure evolves from O' -type orthorhombic to quasitetragonal symmetry. The structural and magnetic properties strongly support tetravalent or nearly tetravalent state for Ce in this system. The lower Ce substitution ($x=0.03$ and 0.05) induces sharp and strongly correlated metamagnetic and electronic transitions at low temperatures, as a result of an enhanced $\text{Mn}^{3+/4+}$ ratio and σ^2 . For higher Ce substitution ($x \geq 0.1$), the system is driven to a spin-glass-like state. The magnetoresistance implies the opening of the conducting channels at high magnetic fields in the $\text{Pr}_{0.4}\text{Ce}_{0.1}\text{Ca}_{0.5}\text{MnO}_3$ compound, which shows spin-glass-like behavior. A detailed neutron diffraction study may throw more light on the complex magnetic structure of these compounds.

-
- ¹ *Colossal Magnetoresistance*, edited by C. N. R. Rao and B. Raveau (World Scientific, Singapore, 1998).
- ² E. Dagotto, T. Hotta, and A. Moreo, *Phys. Rep.* **344**, 1 (2001).
- ³ Y. Tokura and Y. Tomioka, *J. Magn. Magn. Mater.* **200**, 1 (1999).
- ⁴ Lide M. Rodriguez-Martinez and J. P. Attfield, *Phys. Rev. B* **54**, R15622 (1996); **58**, 2426 (1998); **63**, 024424 (2000).
- ⁵ Y. Tomioka, A. Asamitsu, Y. Moritomo, H. Kuwahara, and Y. Tokura, *Phys. Rev. Lett.* **74**, 5108 (1995).
- ⁶ V. Kiryukhin, D. Casa, J. P. Hill, B. Keimer, A. Vigliante, Y. Tomioka, and Y. Tokura, *Nature (London)* **386**, 813 (1997).
- ⁷ V. Kiryukhin, Y. J. Wang, F. C. Chou, M. A. Kastner, and R. J. Birgeneau, *Phys. Rev. B* **59**, R6581 (1999).
- ⁸ K. Miyano, T. Tanaka, Y. Tomioka, and Y. Tokura, *Phys. Rev. Lett.* **78**, 4257 (1997).
- ⁹ M. Tokunaga, N. Miura, Y. Tomioka, and Y. Tokura, *Phys. Rev. B* **57**, 5259 (1998), and references therein.
- ¹⁰ R. Mahendiran, A. Maignan, S. Hébert, C. Martin, M. Hervieu, B. Raveau, J. F. Mitchell, and P. Schiffer, *Phys. Rev. Lett.* **89**, 286602 (2002).
- ¹¹ B. Raveau, D. Zhu, A. Maignan, M. Hervieu, C. Martin, V. Hardy, and S. Hébert, *J. Phys.: Condens. Matter* **15**, 7055 (2003).
- ¹² K. R. Mavani and P. L. Paulose, *Appl. Phys. Lett.* **86**, 162504 (2005); *Solid State Commun.* **135**, 183 (2005).
- ¹³ V. Hardy, S. Hébert, A. Maignan, C. Martin, M. Hervieu, and B. Raveau, *J. Magn. Magn. Mater.* **264**, 183 (2003).
- ¹⁴ F. M. Woodward, J. W. Lynn, M. B. Stone, R. Mahendiran, P. Schiffer, J. F. Mitchell, D. N. Argyriou, and L. C. Chapon, *Phys. Rev. B* **70**, 174433 (2004).
- ¹⁵ Yukitoshi Motome, Nobuo Furukawa, and Naoto Nagaosa, *Phys. Rev. Lett.* **91**, 167204 (2003).
- ¹⁶ C. Sen, G. Alvarez, and E. Dagotto, *Phys. Rev. B* **70**, 064428 (2004).
- ¹⁷ H. Aliaga, D. Magnoux, A. Moreo, D. Poilblanc, S. Yunoki, and E. Dagotto, *Phys. Rev. B* **68**, 104405 (2003).
- ¹⁸ R. Mathieu, D. Akahoshi, A. Asamitsu, Y. Tomioka, and Y. Tokura, *Phys. Rev. Lett.* **93**, 227202 (2004).
- ¹⁹ A. Sundaresan, V. Caignaert, A. Maignan, B. Raveau, and E. Suard, *Phys. Rev. B* **60**, 533 (1999).
- ²⁰ Z. Zeng, M. Greenblatt, and M. Croft, *Phys. Rev. B* **63**, 224410 (2001).
- ²¹ J.-S. Kang, Y. J. Kim, B. W. Lee, C. G. Olson, and B. I. Min, *J. Phys.: Condens. Matter* **13**, 3779 (2001).
- ²² E. N. Caspi, M. Avdeev, S. Short, J. D. Jorgensen, M. V. Lobanov, Z. Zeng, M. Greenblatt, P. Thiyagarajan, C. E. Botez, and P. W. Stephens, *Phys. Rev. B* **69**, 104402 (2004).
- ²³ M. S. Kim, J. B. Yang, Q. Cai, X. D. Zhou, W. J. James, W. B. Yelon, P. E. Parris, D. Buddhikot, and S. K. Malik, *Phys. Rev. B* **71**, 014433 (2005).
- ²⁴ M. R. Lees, J. Baratt, G. Balakrishnan, D. McK Paul, and C. D. Dewhurst, *J. Phys.: Condens. Matter* **8**, 2967 (1996).
- ²⁵ B. Raveau, A. Maignan, and C. Martin, *J. Solid State Chem.* **130**, 162 (1997).
- ²⁶ R. Mahendiran, M. Hervieu, A. Maignan, C. Martin, and B. Raveau, *Solid State Commun.* **114**, 429 (2000).
- ²⁷ A. Sundaresan, A. Maignan, and B. Raveau, *Phys. Rev. B* **56**, 5092 (1997).
- ²⁸ J. M. De Teresa, M. R. Ibarra, J. Garcia, J. Blasco, C. Ritter, P. A. Algarabel, C. Marquina, and A. del Moral, *Phys. Rev. Lett.* **76**, 3392 (1996).
- ²⁹ J. Blasco, C. Ritter, J. Garcia, J. M. de Teresa, J. Perez-Cacho, and M. R. Ibarra, *Phys. Rev. B* **62**, 5609 (2000).
- ³⁰ J. Burgy, M. Mayr, V. Martin-Mayor, A. Moreo, and E. Dagotto, *Phys. Rev. Lett.* **87**, 277202 (2001).